

## Electronic Supplementary Information

### Efficient photocatalytic hydrogen evolution based on Z-scheme 2D LaVO<sub>4</sub>/ 2D Mo-doped S<sub>V</sub>-ZnIn<sub>2</sub>S<sub>4</sub> heterojunction

Wei Guan,<sup>1</sup> Lin Zhang,<sup>1</sup> Peng Wang,<sup>1</sup> Ying Wang,<sup>1</sup> Haoyu Wang,<sup>1</sup> Xingchen Dong,<sup>1</sup> Liyan Yu<sup>1</sup>,

Zhixing Gan<sup>1,2\*</sup>, Lifeng Dong<sup>1\*</sup> and Lina Sui<sup>1\*</sup>

<sup>1</sup> College of Materials Science and Engineering, Qingdao University of Science and Technology, Qingdao, 266042, PR China.

<sup>2</sup> Center for Future Optoelectronic Functional Materials, School of Computer and Electronic Information/School of Artificial Intelligence, Nanjing Normal University, Nanjing 210023, PR China.

\*Correspondence and requests for materials should be addressed to Z.G., L.D. or L. S.

(E-mail: [zxgan@njnu.edu.cn](mailto:zxgan@njnu.edu.cn) or [donglifeng@qust.edu.cn](mailto:donglifeng@qust.edu.cn) or [linasui@qust.edu.cn](mailto:linasui@qust.edu.cn))

## Methods

### Materials.

Analytical grade reagents were used directly without purification.  $\text{LaN}_3\text{O}_9 \cdot 6\text{H}_2\text{O}$  (99.99%),  $\text{NH}_4\text{VO}_3$  (99.9%),  $\text{InCl}_3$  (99.99%),  $\text{Na}_2\text{MoO}_4$  (99.99%),  $\text{Zn}(\text{CH}_3\text{COO})_2 \cdot 2\text{H}_2\text{O}$  (99.8%), Thioacetamide (TAA, 99%), Triethanolamine (TEOA, 98%) were obtained from Shanghai Aladdin Ltd. NaOH (99%), Cyclohexane (99%), Oleic acid (99%), Anhydrous ethanol (99%) were purchased from Sinopharm Chemical Reagent Co., Ltd.

### Synthesis of ZIS.

The ZIS was prepared by a hydrothermal method, 1.6 mmol  $\text{Zn}(\text{CH}_3\text{COO})_2 \cdot 2\text{H}_2\text{O}$ , 3.2 mmol  $\text{InCl}_3$ , and 6.4 mmol TAA were dispersed in 30 mL deionized water and 30 mL ethanol with vigorous stirring for 30 min. Then, the obtained solution was transferred into a 100 mL Teflon-lined autoclave and heated at 180 °C for 24 h. The sample was washed with deionized water and ethanol several times and then vacuum-dried.

### Synthesis of $\text{S}_V\text{-MZIS}$

The synthesis process of  $\text{S}_V\text{-MZIS}$  is the same as that of ZIS. 0.03mmol  $\text{Na}_2\text{MoO}_4$ , 1.6 mmol  $\text{Zn}(\text{CH}_3\text{COO})_2 \cdot 2\text{H}_2\text{O}$ , 3.2 mmol  $\text{InCl}_3$ , and 12.8 mmol TAA were dispersed in 30 mL deionized water and 30 mL ethanol with vigorous stirring for 30 min. Then, the obtained solution was transferred into a 100 mL Teflon-lined autoclave and heated at 180 °C for 24 h. The sample was washed with deionized water and ethanol several times and then vacuum-dried.

### **Synthesis of LaVO<sub>4</sub>**

LaVO<sub>4</sub> was synthesized by solvothermal method. 1.2 g NaOH and 0.12 g NH<sub>4</sub>VO<sub>3</sub> were added to 10 mL of deionized water, then 20 mL of oleic acid and 20 mL of anhydrous ethanol were added sequentially with vigorous stirring for 30 min. 2 mL (1 mmol/mL) of aqueous La(NO<sub>3</sub>)<sub>3</sub>·6H<sub>2</sub>O solution was then added. The mixed solution was transferred to a 100 mL Teflon reactor and kept at 140 °C for 8 h. After natural cooling to room temperature, the sample was washed with cyclohexane and ethanol several times. Finally, the obtained LaVO<sub>4</sub> nanosheets were placed in a vacuum drying oven at 60 °C for 6 h.

### **Synthesis of V-LaVO<sub>4</sub>**

200 mg of LaVO<sub>4</sub> was taken into a crucible and calcined in a tube furnace at 450°C in the air for 4 h. Finally, V-LaVO<sub>4</sub> was obtained.

### **Synthesis of R-LaVO<sub>4</sub>**

200 mg of V-LaVO<sub>4</sub> was taken and dispersed in a solution consisting of 20 mL of N<sub>2</sub>H<sub>4</sub>·H<sub>2</sub>O and 40 mL of deionized water, stirred for 30 min. Transferred to a 100 mL Teflon reactor and kept at 240°C for 5 h. The sample was washed with deionized water several times and then vacuum-dried. Finally obtained R-LaVO<sub>4</sub>.

### **Synthesis of R-LaVO<sub>4</sub>/ S<sub>V</sub>-MZIS**

The synthesis process of R-LaVO<sub>4</sub>/ S<sub>V</sub>-MZIS is the same as that of S<sub>V</sub>-MZIS. An amount of R-LaVO<sub>4</sub> was added to the precursor solution of S<sub>V</sub>-MZIS and stirred for 30 min, then transferred to a 100 mL Teflon lined reactor and kept at 180 °C for 24 h. The

sample was washed with deionized water and ethanol several times and then vacuum-dried.

## **Characterizations**

X-ray diffraction (XRD) patterns were examined by a Bruker D8 diffractometer using Cu Ka radiation. The morphologies and microstructures of the samples were characterized by a transmission electron microscope (TEM, FEI, JEM-2100PLUS, JP). Atomic force microscopy (AFM, AFM5000II) was used to examine the micromorphology. Brunauer Emmett Teller (BET) surface area was tested with an automatic instrument (ASAP 2460, Micromeritics, USA). Raman was tested with Raman Spectrometer (Invia Qontor, Renishaw, UK). Fourier Transform Infrared (FT-IR) was tested with Fourier Transform infrared spectroscopy (Nicolet IS10, Thermo, USA). Droplet contact Angle was tested with a contact Angle measuring instrument (LSA100, LAUDA, DE). X-ray photoelectron spectroscopy (XPS) was used to analyse the structure and composition of the samples by Thermo ESCALAB 250Xi with Al Ka source. The XPS spectra were calibrated through the standard C 1s peak at 284.8 eV. Ultraviolet–visible diffuse reflectance (UV–vis) spectra in the range of 200-800 nm were recorded by a spectrophotometer (Cary5000, Varian, USA). Free radicals and vacancy were explored by electron spin resonance spectra (EPR, EPR200-Plus, CN). The surface photovoltage (SPV) was measured by the surface photovoltage spectrometer (CEL-SPS1000, Beijing China Education Au-light Co. Ltd. China).

## **Photoelectrochemical measurements**

Electrochemical measurements were performed using an electrochemical analyser (Autolab, PGSTAT 302 N) with a standard three-electrode system. 0.5 M Na<sub>2</sub>SO<sub>4</sub> solution was used as the electrolyte for transient photocurrent and electrochemical impedance spectroscopy (EIS) measurements. The photocatalysts were coated on fluorine-doped tin oxide (FTO) glass with an area of 1 cm<sup>2</sup> in a three-electrode system. Platinum sheets and Ag/AgCl were used as counter and reference electrodes, respectively. Typically, 6 mg of catalyst was dispersed in 300 μL deionized water, which was then dropped evenly on the FTO glass and dried on a hot plate to ensure that the samples were snug on the FTO substrate. EIS was performed over a frequency range of 0.01 Hz to 100 kHz with an AC amplitude of 100 mV. Transient photocurrents were tested with illumination (300 W Xe lamp, 1.5 adaptive median (AM) filter) at 0.1 V bias.

### **Photocatalytic hydrogen evolution**

Photocatalytic water splitting reaction over the photocatalysts was conducted in a Pyrex top-irradiation reaction vessel connected to a closed glass gas circulation system with cooling water (6 °C) to maintain the reaction solution. Typically, 10 mg of photocatalyst powder was dispersed in 50 mL aqueous solution containing 10 vol% triethanolamine sacrificial agent. Before the test, the prepared suspension was evacuated for 30 min to completely remove the dissolved oxygen. A 300 W Xe lamp with a 420 nm cut-off filter was used as the visible light source. The amount of hydrogen evolution was analysed by a gas chromatographer (GC7920, Beijing China Education Au-light Co. Ltd. China). The apparent quantum yield (AQY) for hydrogen

evolution was measured under illumination of the simulated solar light with a band-pass filter (380, 420, 550 nm). Photon flux of the incident light was measured using an optical power meter (CEL-NP2000, Beijing China Education Au-Light Co., Ltd). The AQY was calculated according to the following equation:

$$AQY(\%) = \frac{N_e}{N_p} = \frac{2 \times \text{number of evolved } H_2 \text{ molecules}}{\text{number of incident photons}} \times 100\%$$

$$= \frac{2 \times nH_2 \times N_A \times h \times c}{S \times P \times t \times \lambda} \times 100\%$$

where  $N_p$  is the total incident photons,  $N_e$  is the total reactive electrons,  $M$  is the amount of  $H_2$  molecules,  $N_A$  is Avogadro constant,  $h$  is Planck's constant,  $c$  is the speed of light,  $S$  is the irradiation area,  $P$  is the intensity of irradiation light,  $t$  is the photoreaction time, and  $\lambda$  is the wavelength of the monochromatic light.

## Calculation methods

The calculation adopted density functional theory (DFT) combined with mode conservation pseudopotential and plane wave method in CASTEP program of Materials Studio. The conjugate gradient method was to minimize the total energy of the system to obtain a self-consistent ground state of the system. In the self-consistent field calculation, the electronic wave function of the system was obtained by the Pulay density mixing method. The Broyden, Fletcher, Goldfarb and Shannon (BFGS) methods were used to optimize the structure of the system. The generalized gradient approximation (GGA) and Perdew-Burke-Ernzerhof (PBE) functional combined. The plane wave cutoff energy was 500 eV. The Monkhorst Pack method was used to sample the Brillouin area, and the k-point grid was  $3 \times 3 \times 1$ . In the process of structural

optimization, the total energy convergence criterion of the system was  $1.0 \times 10^{-5}$  eV, the residual force convergence criterion was  $0.03 \text{ eV} \times \text{\AA}^{-1}$ , the atomic displacement convergence criterion was  $1.0 \times 10^{-3}$  \AA, and the volume stress convergence criterion was 0.05 GPa. The cutoff energy of the plane wave and the value of the k-point grid ensured the convergence of the total energy of the system.

The free energy change ( $\Delta G$ ) for adsorptions were determined as follows:

$$\Delta G = E_{\text{total}} - E_{\text{sur}} - E_{\text{H}} + \Delta E_{\text{ZPE}} - T\Delta S$$

where  $E_{\text{total}}$  is the total energy for the adsorption state,  $E_{\text{sur}}$  is the energy of pure surface,  $E_{\text{H}}$  is the energy of H,  $\Delta E_{\text{ZPE}}$  is the zero-point energy change and  $\Delta S$  is the entropy change. As the vibrational entropy of  $\text{H}^*$  in the adsorbed state is small, the entropy of adsorption of  $1/2 \text{ H}_2$  is  $S_{\text{H}} \approx -0.5S_{\text{H}_2}$ , where  $S_{\text{H}_2}$  is the entropy of  $\text{H}_2$  in the gas phase at the standard conditions. Therefore, the overall corrections were taken as in

$$\Delta G_{\text{H}^*} = E_{\text{total}} - E_{\text{sur}} - E_{\text{H}_2}/2 + 0.24 \text{ eV}$$

where  $E_{\text{H}_2}$  is the energy of  $\text{H}_2$  in gas phase.

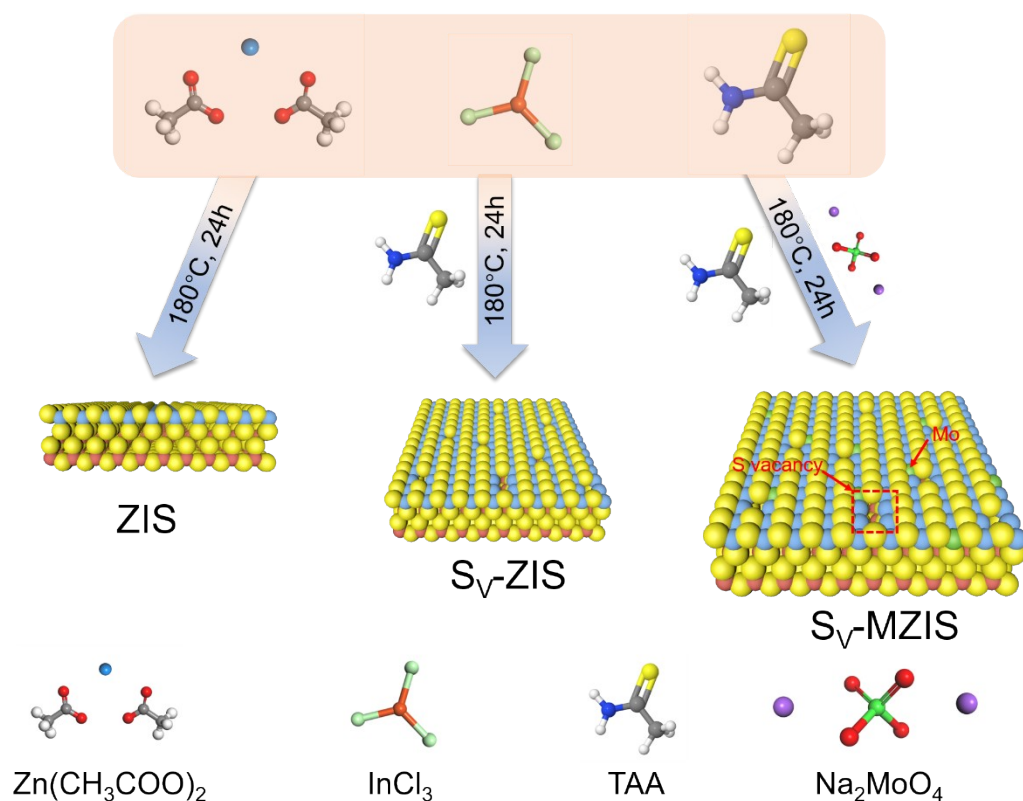


Fig. S1. Schematic diagram illustrating the synthesis of ZIS, S<sub>V</sub>-ZIS, and S<sub>V</sub>-MZIS.

As shown in Fig. S1, ZIS containing sulfur vacancies (S<sub>V</sub>-ZIS) was obtained by adding an excess of TAA, which can adsorb on the surface of primary ZIS crystals and inhibit crystal growth, thus creating sulfur vacancies<sup>1, 2</sup>. Molybdenum doped S<sub>V</sub>-ZIS (S<sub>V</sub>-MZIS) was obtained by the addition of Na<sub>2</sub>MoO<sub>4</sub>. Since the atomic size of the molybdenum atom (1.40 Å) is similar to that of the Zn atom (1.39 Å), the molybdenum atom can enter the ZIS lattice by taking the place of the Zn atom to obtain S<sub>V</sub>-MZIS, as demonstrated in our previous work<sup>3, 4</sup>.

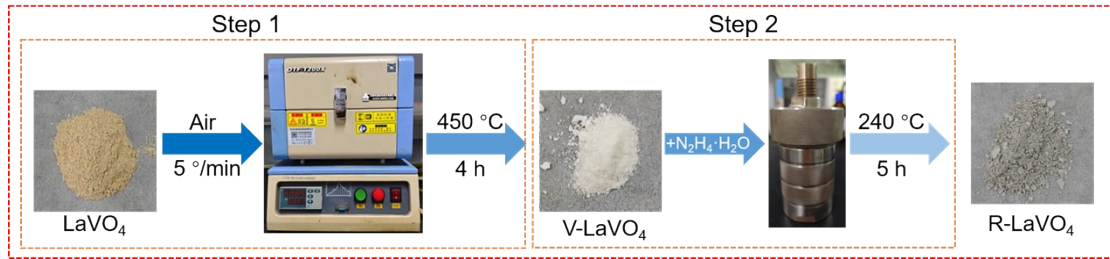


Fig. S2. Schematic diagram illustrating the synthesis of  $\text{V-LaVO}_4$ , and  $\text{R-LaVO}_4$ .

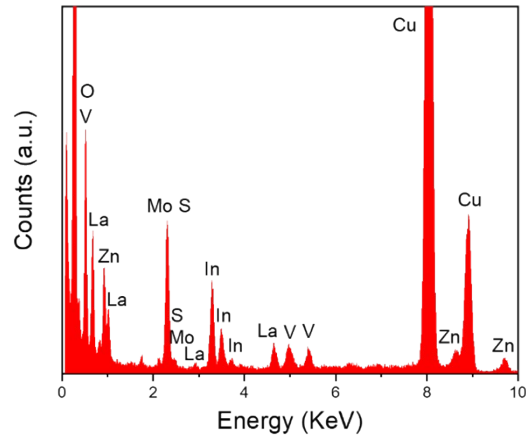


Fig. S3. EDX of the  $7\% \text{R-LaVO}_4/\text{S}_\text{V}\text{-MZIS}$  shows the presence of Mo, Zn, In, S, La, V, and O.

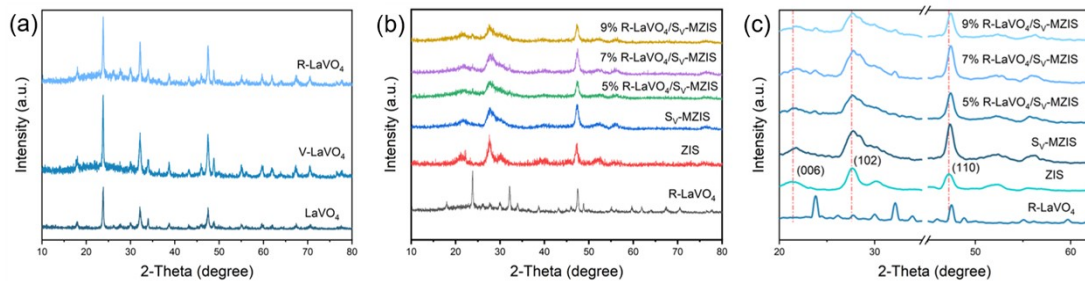


Fig. S4. (a) XRD patterns of  $\text{LaVO}_4$ ,  $\text{V-LaVO}_4$ , and  $\text{R-LaVO}_4$ . (b, c) Raw XRD patterns of  $\text{R-LaVO}_4$ , ZIS,  $\text{S}_\text{V}\text{-MZIS}$ , and  $X\% \text{R-LaVO}_4/\text{S}_\text{V}\text{-MZIS}$  ( $X=5, 7, 9$ ).

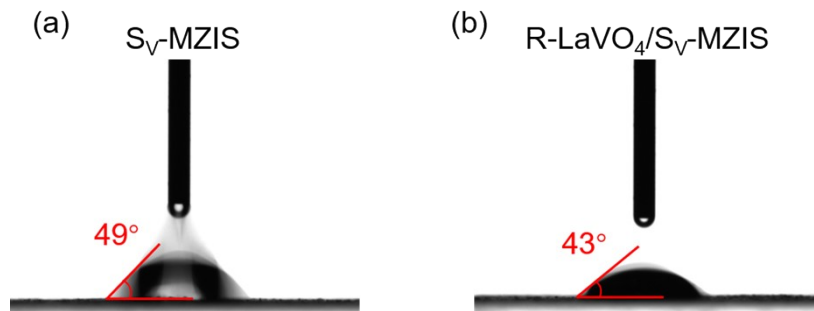


Fig. S5. (a, b) Water-droplet contact angles of  $\text{S}_\text{V}\text{-MZIS}$  (a), and  $\text{R-LaVO}_4/\text{S}_\text{V}\text{-MZIS}$  (b).

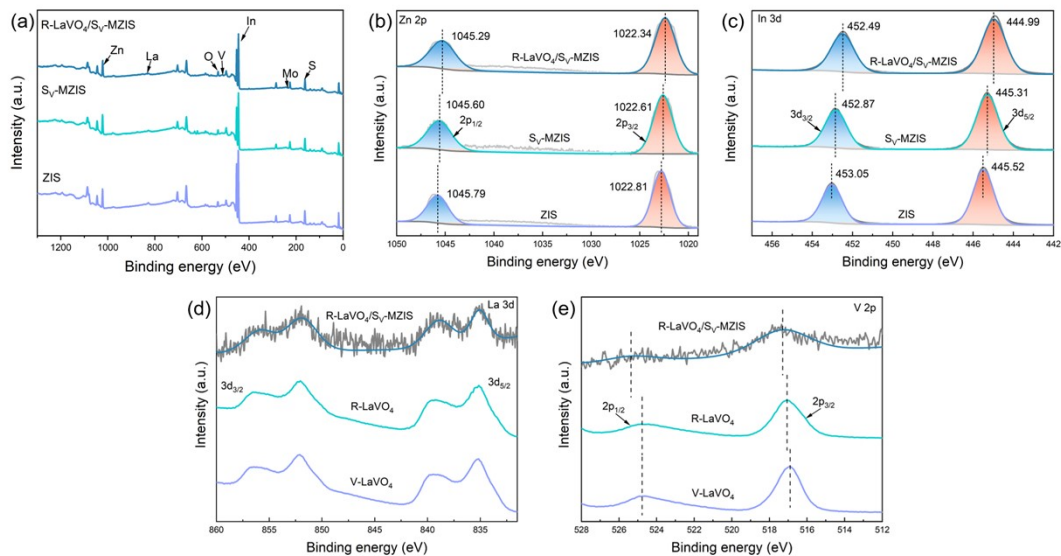


Fig. S6. (a) Full survey XPS spectra of ZIS,  $S_V$ -MZIS, and 7% R-LaVO<sub>4</sub>/ $S_V$ -MZIS. (b, c) Zn 2p (b), In 3d (c) XPS spectra of ZIS,  $S_V$ -MZIS, and 7% R-LaVO<sub>4</sub>/ $S_V$ -MZIS. (d, e) V 2p (d), La 3d (e) XPS spectra of V-LaVO<sub>4</sub>, R-LaVO<sub>4</sub>, and 7% R-LaVO<sub>4</sub>/ $S_V$ -MZIS.

As shown in Fig. S6b, Zn 2p<sub>3/2</sub> and Zn 2p<sub>1/2</sub> of  $S_V$ -MZIS are located at 1022.61 and 1045.60 eV, respectively, and the binding energies are significantly lower than those of ZIS (1022.81 eV and 1045.79 eV). Fig. S6c shows the binding energies of In 3d<sub>5/2</sub> and In 3d<sub>3/2</sub> of  $S_V$ -MZIS are 445.31 and 452.87 eV, respectively, and the binding energies of  $S_V$ -MZIS are significantly lower than those of ZIS (445.52 and 453.05 eV), indicating that the coordination number of Zn and In is reduced, proving that there are sulfur vacancies in  $S_V$ -MZIS. As shown in Fig. S6d and S6e, the peak signals of 2p<sub>1/2</sub> and 2p<sub>3/2</sub> for V 2p and 3d<sub>3/2</sub> and 3d<sub>5/2</sub> for La 3d are observed in the V 2p and La 3d spectra, respectively. After complexation with  $S_V$ -MZIS, the peak signals of 2p<sub>1/2</sub> and 2p<sub>3/2</sub> of V 2p and 3d<sub>3/2</sub> and 3d<sub>5/2</sub> of La 3d are still observed in the V 2p and La 3d spectra, demonstrating the successful complexation of R-LaVO<sub>4</sub> and  $S_V$ -MZIS.

Table. S1. Elemental compositions of  $\text{LaVO}_4$ ,  $\text{V-LaVO}_4$ , and  $\text{R-LaVO}_4$  according to XPS.

Element	La(%)	V(%)	O(%)	La : V : O
$\text{LaVO}_4$	17.39	13.28	69.33	1:0.76:3.99
$\text{V-LaVO}_4$	19.34	13.47	67.19	1:0.69:3.47
$\text{R-LaVO}_4$	18.93	14.11	66.96	1:0.75:3.53

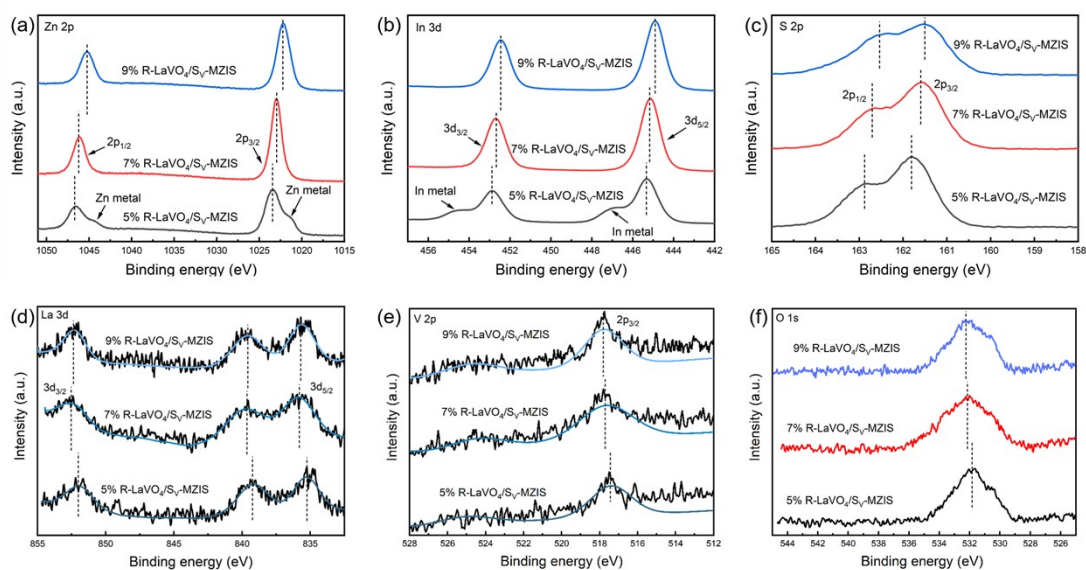


Fig. S7. XPS spectra of 5%, 7%, and 9%  $\text{R-LaVO}_4/\text{S}_v\text{-MZIS}$ . (a) Zn 2p, (b) In 3d, (c) S 2p (d) La 3d, (e) V 2p, (f) O 1s.

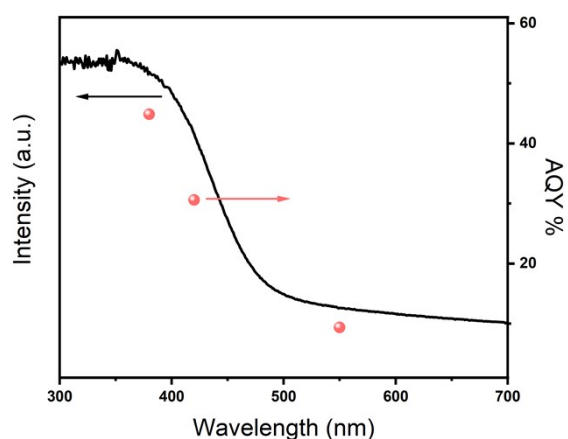


Fig. S8. wavelength-dependent apparent quantum yield (AQY).

Photocatalytic hydrogen evolution AQY calculation process:

$$AQY(\%) = \frac{N_e}{N_p} = \frac{2 \times \text{number of evolved } H_2 \text{ molecules}}{\text{number of incident photons}} \times 100\% = \frac{2 \times nH}{S \times t} \times 100\%$$

When  $\lambda = 420 \text{ nm}$

$$AQY = \frac{2 \times 144.8 \times 10^{-6} \times 6.022 \times 10^{23} \times 6.626 \times 10^{-34} \times 3 \times 10^8}{0.075 \times 3600 \times 420 \times 10^{-9}} \times 100\% = 30.57\%$$

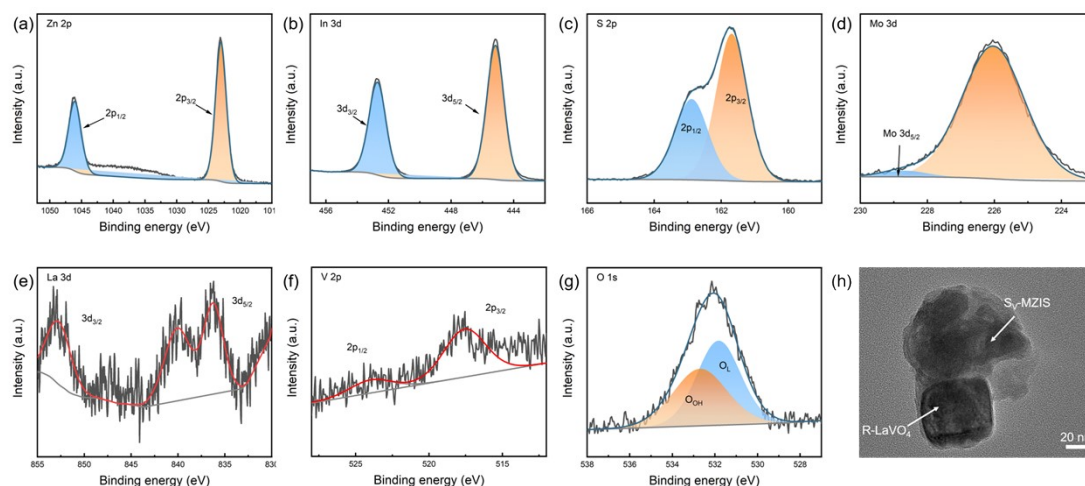


Fig. S9. XPS spectra of R-LaVO<sub>4</sub>/S<sub>V</sub>-MZIS after photocatalytic test. (a) Zn 2p, (b) In 3d, (c) S 2p (d) Mo 3d, (e) La 3d, (f) V 2p, (g) O 1s. (h) TEM image of R-LaVO<sub>4</sub>/S<sub>V</sub>-MZIS after photocatalytic test.

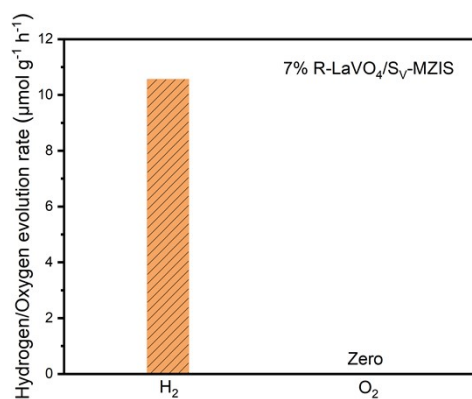


Fig. S10. Photocatalytic water overall splitting over 7% R-LaVO<sub>4</sub>/S<sub>V</sub>-MZIS.

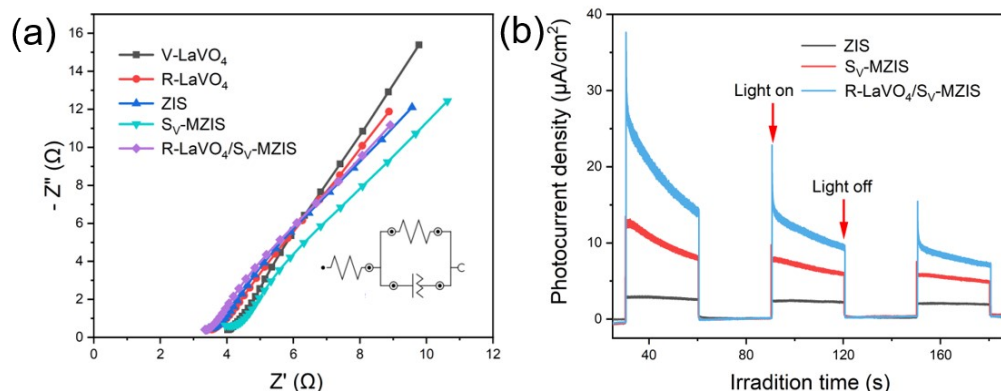


Fig. S11. (a) EIS plots of V-LaVO<sub>4</sub>, R-LaVO<sub>4</sub>, ZIS, S<sub>V</sub>-MZIS, and 7% R-LaVO<sub>4</sub>/S<sub>V</sub>-MZIS. (b) Photocurrent response of ZIS, S<sub>V</sub>-MZIS, and 7% R-LaVO<sub>4</sub>/S<sub>V</sub>-MZIS. During the test, the catalyst falls off the FTO glass, resulting in a reduction in the amount of catalyst effectively tested. Thus, the photocurrent density decreases over time, which is not related to the stability of the photocatalyst.

Table. S2. Impedance values of V-LaVO<sub>4</sub>, R-LaVO<sub>4</sub>, ZIS, S<sub>V</sub>-MZIS, and 7% R-LaVO<sub>4</sub>/S<sub>V</sub>-MZIS obtained by fitting on the EIS results.

Sample	V-LaVO <sub>4</sub>	R-LaVO <sub>4</sub>	ZIS	S <sub>V</sub> -MZIS	R-LaVO <sub>4</sub> /S <sub>V</sub> -MZIS
R <sub>S</sub>	4.28 Ω	3.71 Ω	3.56 Ω	4.17 Ω	3.38 Ω
R <sub>ct</sub>	95.74 Ω	84.04 Ω	130.77 Ω	104.56 Ω	72.55 Ω

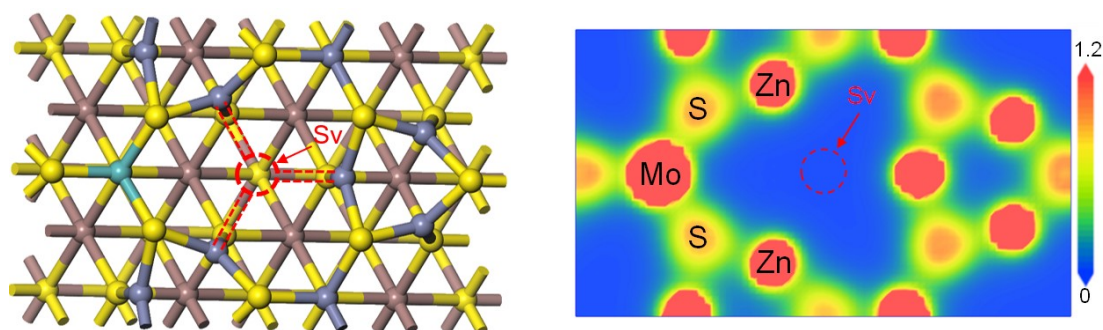


Fig. S12. (a) Crystal structure diagram of S<sub>V</sub>-MZIS. (b) Electron difference density of S<sub>V</sub>-MZIS.

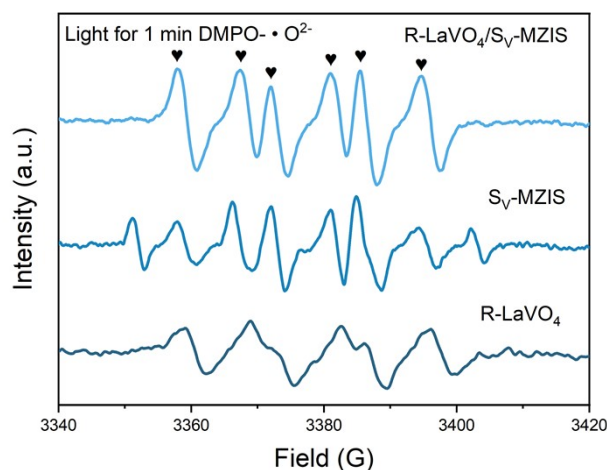


Fig. S13. DMPO spin-trapping electron paramagnetic resonance (EPR) spectra of DMPO-•O<sup>2-</sup> of R-LaVO<sub>4</sub>, S<sub>V</sub>-MZIS, and R-LaVO<sub>4</sub>/S<sub>V</sub>-MZIS.

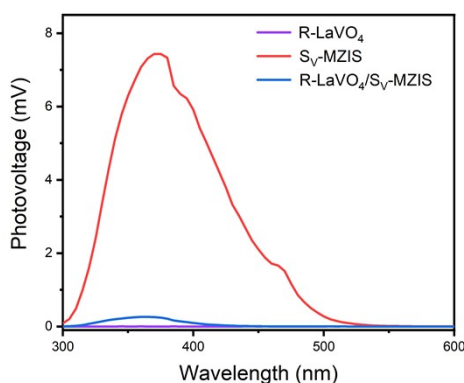


Fig. S14. Surface photovoltage (SPV) spectra of R-LaVO<sub>4</sub>, S<sub>V</sub>-MZIS, and R-LaVO<sub>4</sub>/S<sub>V</sub>-MZIS.

## References

1. C. Du, Q. Zhang, Z. Lin, B. Yan, C. Xia and G. Yang, *Applied Catalysis B: Environmental*, 2019, **248**, 193-201.
2. J. Xie, H. Zhang, S. Li, R. Wang, X. Sun, M. Zhou, J. Zhou, X. W. Lou and Y. Xie, *Adv Mater*, 2013, **25**, 5807-5813.
3. W. Guan, L. Zhang, P. Wang, Y. Wang, H. Wang, X. Dong, M. Meng, L. Sui, Z. Gan, L. Dong and L. Yu, *Nanomaterials*, 2022, **12**, 3980.
4. W. Guan, R. Jia, L. Zhang, M. Meng, P. Wang, Y. Wang, H. Wang, X. Dong, L. Sui, Z. Gan, L. Dong and L. Yu, *J Colloid Interface Sci*, 2023, **649**, 685-693.